# Substrate-supported large-band-gap quantum spin Hall insulator based on III-V bismuth layers

J. E. Padilha,[1,*] A. Janotti,[2,†] A. Fazzio,[3,4,‡] and A. J. R. da Silva[3,5,§]

[1]*Campus Avançado Jandaia do Sul, Universidade Federal do Paraná, 86900-000 Jandaia do Sul, PR, Brazil*

[2]*Department of Materials Science & Engineering, University of Delaware, Newark, Delaware 19716-3106, USA*

[3]*Instituto de Física, Universidade de São Paulo, C.P. 66318, 05315-970 São Paulo, SP, Brazil*

[4]*Centro de Ciências Naturais e Humanas, Universidade Federal do ABC, Santo André, 09210-170 São Paulo, SP, Brazil*

[5]*Laboratório Nacional de Luz Síncrotron, 13083-100 Campinas, SP, Brazil*

(Received 4 August 2016; revised manuscript received 30 September 2016; published 16 November 2016)

We show that III-V bismuth-based two-dimensional (2D) materials grown on an anion-terminated SrTe (111) substrate are 2D topological insulators. The III-Bi layers exhibit large nontrivial band gaps, ranging from 0.15 to 0.72 eV, depending on the passivation on the top surface, i.e., using hydrogen or halogens. We find that Γ-centered Dirac helical states, protected by time-reversal symmetry, appear at the edges of nanoribbon structures made of III-Bi layers on the SrTe substrate. The nontrivial character of the band gap is also determined by calculations of the $Z_2$ invariant. We also find that the topological phase is maintained in the ultrathin quantum well heterostructures SrTe/III-Bi/SrTe, i.e., when the 2D materials are sandwiched between SrTe along the [111] direction, opening a new route for the fabrication of nanostructured devices based on 2D quantum spin Hall insulators.

DOI: 10.1103/PhysRevB.94.195424

## I. INTRODUCTION

Two-dimensional (2D) topological insulators (TIs), also known as quantum spin Hall insulators (QSHIs), are promising materials for spintronics and nanoelectronics. These materials display an insulating bulk and spin-polarized gapless edge states with a conical energy dispersion. The edge states are protected against perturbations, which preserves time reversal symmetry, preventing backscattering. The QSHI phase was first proposed to occur in graphene by Kane and Mele [1]. However, due to the very small spin-orbit-induced band gap in graphene, the QSHI phase is expected to occur only at extremely low temperatures [2,3], making it difficult to probe in a controllable manner.

The QSHI phase was first observed in HgTe/CdTe quantum well structures [4], yet the observed band gap of 5 meV is too small for practical applications. Other materials systems have also been proposed for observation of the QSHI phase, such as silicene (with a gap of 1.9 meV) [5,6], germanene (gap of 29 meV) [6,7], stanene (0.1 eV), and its halogenated forms (up to 0.34 eV) [8]. The spin-orbit interaction is a key feature in TIs, raising interest in heavy elements, such as bismuth, as building blocks of these materials. In fact, Bi is responsible for the high spin-orbit coupling (SOC) that drives the band inversion in $Bi_2Se_3$ and $Bi_2Te_3$ [9–12]. Bismuth layers have also been proposed to present the quantum spin Hall effect [13,14].

Motivated by the use of bismuth as a source of high SOC strength, III-Bi binary compounds have been proposed, by Chuang *et al.* [15], as a new class of large-band-gap 2D quantum spin Hall insulators. Their halogenated form [16–18] and the fluorinated PbX binary compounds proposed by Padilha *et al.* [19], are the 2D topological insulators with the largest nontrivial band gaps, to our knowledge. However, these 2D QSHIs were proposed to exist in a freestanding form, which is quite challenging to achieve in practice. The growth of 2D topological insulators on substrates that preserve their topological properties is yet to be demonstrated and would pave the way to more realistic approaches and practical applications.

Having the 2D material supported on a substrate not only is more practical than 2D freestanding layers, but also could provide new ways to control the topological properties and add flexibility to device design. For instance, the substrate could impose strain on the 2D TI, which allows for tuning the nontrivial band gap in 2D systems [20]. However, there are some requirements for the interaction of the 2D TI with the substrate that must be fulfilled in order to preserve the topological phase: The substrate should have a large band gap, and the band alignment between the substrate and the 2D material should be of type II for an effective separation of the topological states in the TI and the trivial states in the substrate. Furthermore, the substrate should not induce metallic surface states near the Fermi level of the 2D material [21]. These requirements point to highly ionic insulators with very large band gaps as substrates, so that surface states appear only close to the band edges and are readily passivated. In this context, Xu *et al.* [22] have recently shown that stanene can be either a trivial or a quantum spin Hall insulator, depending on the substrate, and that other properties such as Rashba splitting can be controlled by the lattice parameter of the substrate. III-Bi materials were previously proposed to be grown on the Si(111) surface [23,24]. Here we propose the growth of III-Bi ultrathin layers on SrTe. The small lattice mismatch between SrTe and the III-Bi compounds facilitates growth, and the much larger band gap of SrTe, compared to Si, will avoid possible conduction through the substrate material.

In this work we show that III-Bi 2D materials grown on anion-terminated SrTe (111) are 2D topological insulators

*jose.padilha@ufpr.br
†janotti@udel.edu
‡fazzio@if.usp.br
§jose.roque@lnls.br

 

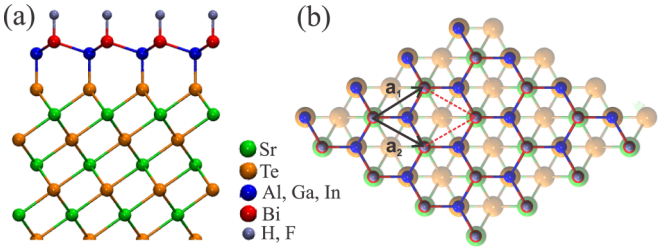


FIG. 1. (a) Side view and (b) top view of the Te-terminated SrTe(111)/III-Bi-X heterostructure, with III: Al, Ga, Bi, and X = H, F, Cl, Br, I. The unit cell is defined by the vectors $\mathbf{a}_1$ and $\mathbf{a}_2$.

when the exposed surface is passivated with hydrogen or halogens. These materials display large nontrivial band gaps, ranging from 0.15 to 0.72 eV. Our calculations show that Γ-centered 1D Dirac helical states, protected by time-reversal symmetry, appear at the edges of III-Bi nanoribbon structures. We also find that there is no interference between the Dirac helical states and the states of the SrTe substrate, which is a trivial insulator with a very large band gap. Finally, we show that when these 2D materials are sandwiched between thick SrTe layers, such as in an ultrathin SrTe/III-Bi/SrTe quantum well heterostructure, the topological phase remains intact. These results open a new route to building nanoscale devices based on 2D quantum spin Hall insulators.

## II. METHODS

Our calculations are based on density functional theory [25–27], as implemented in the VASP code [28]. We use projector augmented wave potentials [29] and a plane-wave basis set with an energy cutoff of 500 eV. The Brillouin zone is sampled with a $9 \times 9 \times 1$ $k$-point mesh. The III-Bi (III = Al, Ga, Bi) layer on the SrTe substrate was simulated using a periodic slab with 15 Å of vacuum. Dipole corrections between the images were included in all calculations. To avoid problems of having different surfaces on the top and bottom of the slab, we employed a symmetric slab, as also used by Xu *et al.* [22] for stanene grown on a substrate. The slabs consisted of 13 atomic layers of substrate, with the inner 7 layers fixed at the bulk crystal structure, and two equivalent top and bottom surfaces covered with III-Bi. Except for the seven inner layers of the SrTe substrate, which were kept fixed during the relaxation process, all other atoms were fully relaxed until the force on each atom was lower than 0.001 eV/Å. Since the materials addressed here do not present inversion symmetry, in order to verify the topological character of the systems, we determine the $Z_2$ invariant based on the evolution of the Wannier center of charges (WCC) method, as

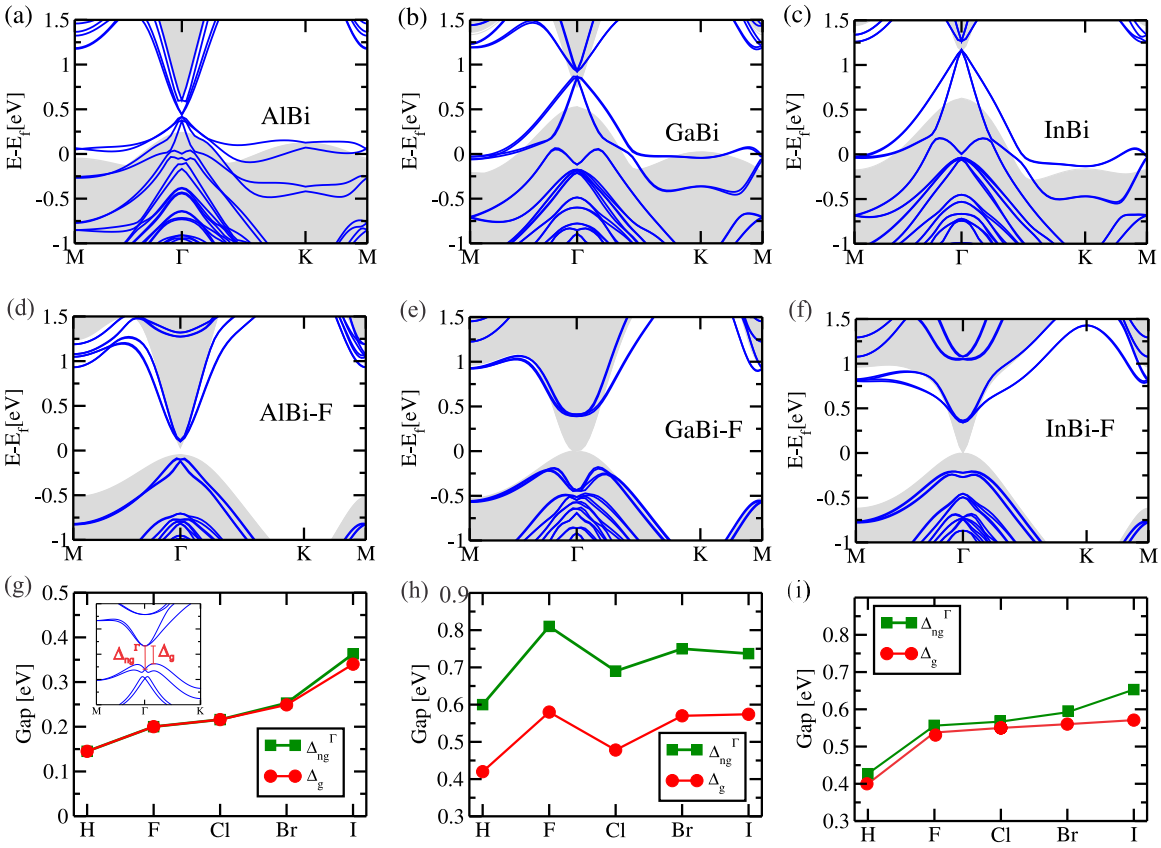


FIG. 2. Band structures of (a) AlBi, (b) GaBi, (c) InBi, (d) AlBi-F, (e) GaBi-F, and (f) InBi-F on Te-terminated SrTe(111). Gray regions represent band structures without spin-orbit coupling (SOC); blue lines, bands with SOC. Evolution of the band gap of III-Bi-X as a function of X (X = H, F, Cl, Br, I) are shown in (g) AlBi-X, (h) GaBi-X, and (i) InBi-X. The metallic, pristine case is not shown. Red circles represent the fundamental band gap ($\Delta_g$) and green squares represent the nontrivial band gap at Γ ($\Delta_{ng}^{\Gamma}$).

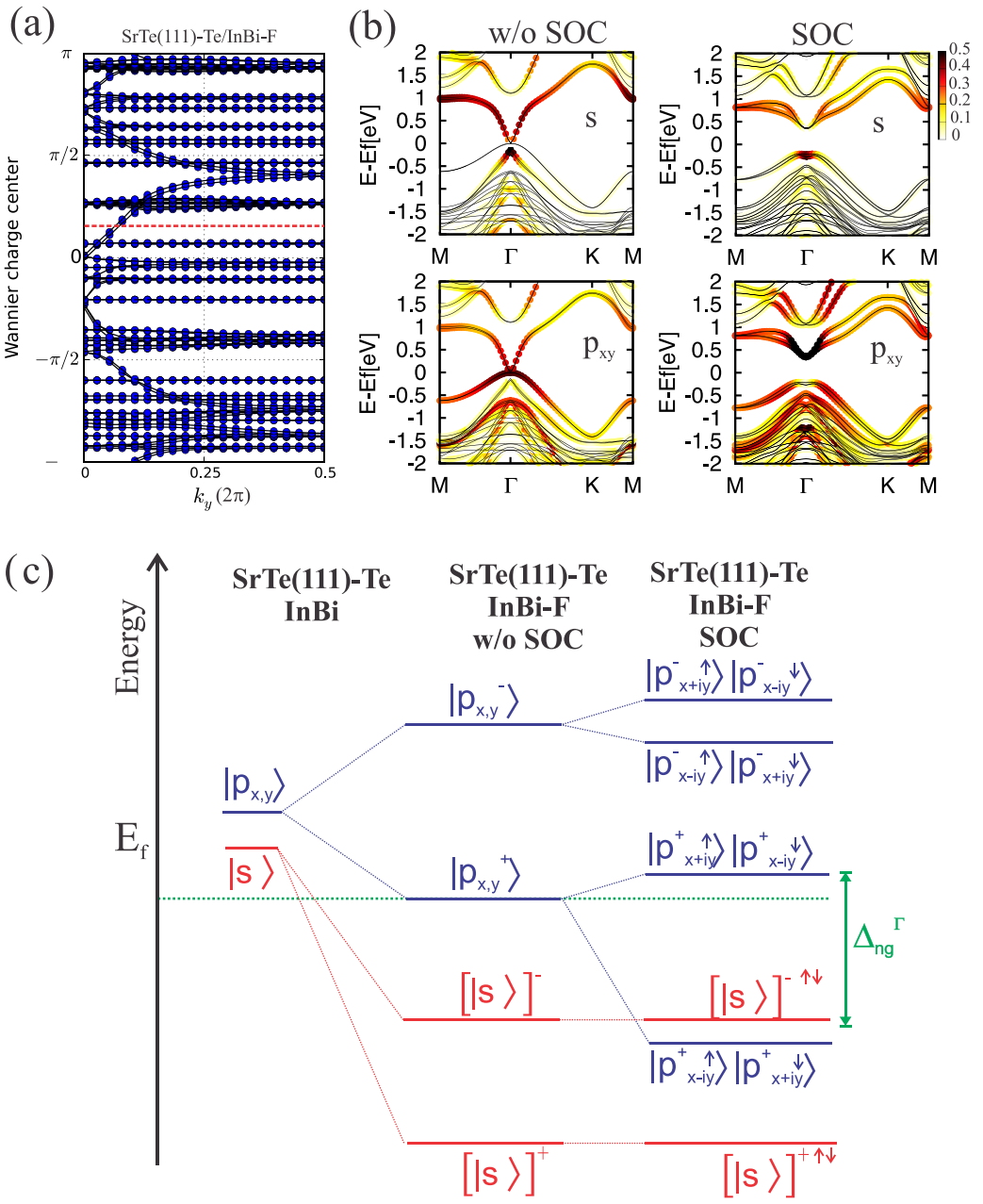


FIG. 3. (a) Tracking of the evolution of the Wannier charge centers (WCCs) between two TRIM points in the reciprocal plane $k_z = 0$. The dashed red horizontal line is a reference to track the number of Wannier center pairs switching in half of the Brillouin zone. (b) Projected band structure of $s$ and $p_{xy}$ orbitals of InBi-F on a Te-terminated SrTe(111) substrate without SOC (left) and with SOC (right). (c) Schematic of the evolution of the $s$ and $p_{xy}$ orbitals for the conduction and valence bands, at the Γ point, of InBi-F on SrTe(111), without and with the SOC.

proposed by Soluyanov and Vanderbilt [30,31]. This method is based on Wannier functions described as

$$|Rn\rangle = \frac{i}{2\pi}\int_{-\pi}^{\pi} dk e^{ik(R-x)}|u_{nk}\rangle \tag{1}$$

The Wannier functions depend on the gauge choice for the Bloch states $|u_{nk}\rangle$. Following Marzari and Vanderbilt's description [32], to optimally localize the Wannier functions, we define the WCC as the mean value of the position operator $\bar{x}_n = \langle 0n|\hat{X}0n\rangle$. In this way $Z_2$ can be written as

$$Z_2 = \left[\sum_{\alpha} \bar{x}_{\alpha}^{I}(\mathrm{TRIM}_1) - \bar{x}_{\alpha}^{II}(\mathrm{TRIM}_1)\right] - \left[\sum_{\alpha} \bar{x}_{\alpha}^{I}(\mathrm{TRIM}_2) - \bar{x}_{\alpha}^{II}(\mathrm{TRIM}_2)\right], \tag{2}$$

where TRIM stands for the time-reversal invariant momentum, $\alpha$ is the band index of the occupied states, and II and I are the Kramer partners. The $Z_2$ invariant can be obtained by

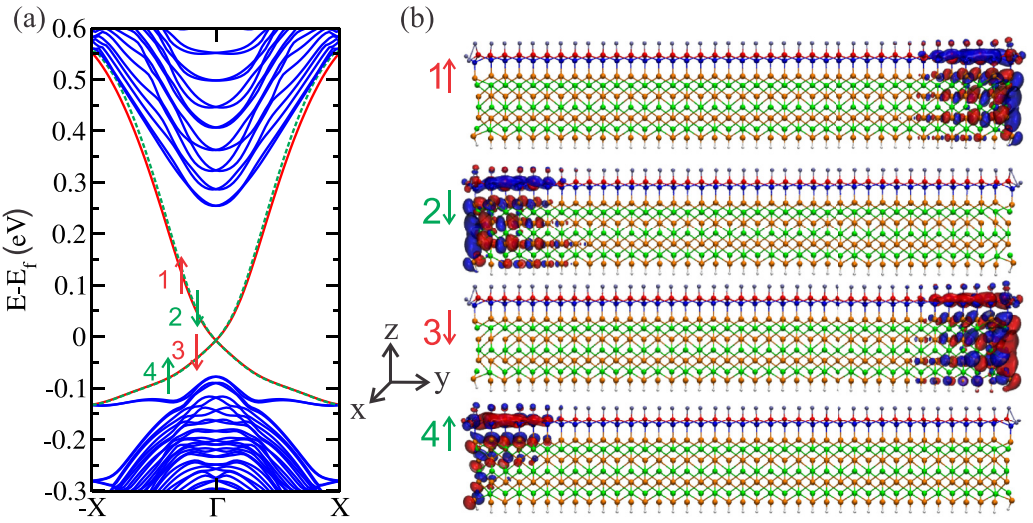


FIG. 4. (a) Electronic band structure of an armchair InBi nanoribbon passivated with fluorine and deposited on top of a Te-terminated SrTe(111) slab. We used a finite slab composed of seven layers of SrTe with InBi-F at the top. On the other side the dangling bonds were saturated with hydrogen atoms to prevent any surface dangling bond states. (b) Wave function for a $k$ point close to the Γ point for each edge state presented in (a).

counting the even or odd number of crossings of any arbitrary horizontal reference line. When the WCC evolution curves cross any arbitrary reference line an odd number of times, $Z_2 = 1$. For ribbon structures, due to the large number of atoms and electrons, we used the OPENMX code [33,34] for band structure calculations since it is more computationally efficient than VASP yet equally accurate.

## III. RESULTS AND DISCUSSION

In Figs. 1(a) and 1(b) we show the side view and top view of the model structure considered in our calculations. As the substrate we used rock salt anion-terminated SrTe(111). SrTe has an experimental lattice parameter of 4.711 Å, which is close to the in-plane lattice parameters of the III-Bi layers [15–18]. In the freestanding form, only the InBi system is mechanically stable, i.e., it has no imaginary modes in the phonon spectra, whereas the Al and Ga materials exhibit low-energy imaginary modes. However, this instability is avoided when the system is grown on a substrate. We find that the lowest-energy configuration for the SrTe/III-Bi interface consists of having the column-III atoms on top of the Te atoms, as shown in Fig. 1, and the Bi atoms on top of the cation site, as in an $hcp$ lattice stacking. We find that the $fcc$ lattice stacking is 0.05 eV higher in energy. Our calculations show that these two interfaces have similar electronic properties. All the other possible configurations are higher in energy.

The band structures of AlBi, GaBi, and InBi on the SrTe substrate are shown in Figs. 2(a), 2(b), and 2(c). The shaded region represents the band structure without SOC, and the blue lines the structure when SOC is turned on. We note that the three systems exhibit a semimetallic character, with the presence of partially occupied states near the Fermi level, around the Γ point. These states are mostly composed of unsaturated $p_z$ orbitals from the Bi atoms in the exposed surface. Adding SOC leads to Rashba-type splitings, however, the metallic character is maintained. In order to remove the unsaturated dangling bond states, we passivate the exposed surface atoms with hydrogen and halogens (F, Cl, Br, and I). We observe that the hydrogen and halogen atoms form strong bonds with the Bi atom, with binding energies varying from ∼3.0 eV for fluorine to ∼2.0 eV for iodine, regardless of the column-III elements. This behavior was also observed for freestanding films [18]. The band structures of the fluorinated surfaces are shown in Figs. 2(d)–2(f). Without SOC, the three materials are semimetals, with the valence and conduction band touching at Γ (shaded region). When SOC is turned on, nontrivial band gaps appear. The variation of the fundamental band gap ($\Delta_g$) and nontrivial band gap ($\Delta_{ng}^{\Gamma}$) with the passivating species X = H, F, Cl, Br, and I is shown in Fig. 2(g) for AlBi, Fig. 2(h) for GaBi, and Fig. 2(i) for InBi. For AlBi, the fundamental band gap and the nontrivial band gap are almost the same for all halogens, except for iodine.

The topological nature of the III-Bi layers can be confirmed by a nonzero topological invariant $Z_2$, calculated here using the WCC method [30,31]. The topological invariant $Z_2 = 1$ was determined for all III-Bi systems, with III = Al, Ga, and Bi, functionalized with H, F, Cl, Br, and I. Only the results for SrTe/InBi-F are shown in Fig. 3(a). By analyzing the evolution of the WCC between two time-reversal-invariant momenta in the Brillouin zone, we find that the WCC always crosses the dashed red line an odd number of times, giving $Z_2 = 1$.

We also verified the topological nature of the band structure by inspecting the orbital-resolved electronic band structure of each material. In Fig. 3(b) we show the orbital-projected band structure of SrTe/InBi-F. The projections on $s$ (top) and $p_{xy}$ (bottom) orbitals without SOC are shown in the left panel, where we note an $s$-$p$ band inversion near the Γ point. When SOC is included, there is an opening of a gap at the Fermi level; the $s$ state remains occupied at the valence band and the $p_{xy}$ states are unoccupied in the conduction band. In Fig. 3(c) we show an energy schematic of SrTe/InBi-F for the electronic states near the Fermi level, with and without SOC.

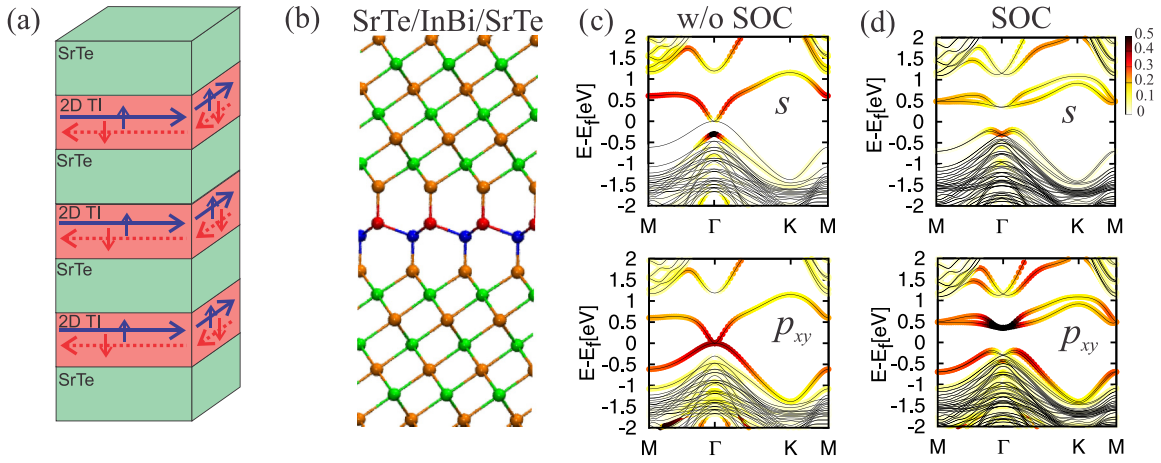


FIG. 5. (a) Schematic of a heterostructure of several 2D TIs grown on substrates. (b) Ball-stick representation of InBi between two SrTe(111) layers. Orbital resolved band structure projected on the $s$ and $p_{xy}$ orbitals of InBi between SrTe (c) without SOC and (d) with SOC.

The unsaturated system is metallic, and the $s$ and $p_{xy}$ states are unoccupied. With the F atoms bonded to the Bi atoms, $s$ states are populated and $p_{xy}$ orbitals are lowered to the Fermi level. When SOC is included, there is a split of the $p_{xy}$ bonding and antibonding states, opening a nontrivial band gap at the Γ point. We have checked that the $s$-$p$ band inversion is preserved when the calculations are performed using the HSE06 hybrid functional calculations [35,36].

A key feature of 2D topological insulators is the existence of an odd number of topologically protected 1D helical Dirac-like edge states. These states connect the conduction and valence bands when the 2D topological insulator is interfaced with a trivial insulator. In Fig. 4(a) we show the band structure for an armchair-terminated nanoribbon with a width of ∼10 nm, where we can clearly see the presence of Dirac-like edge states. The spacial distribution of the Dirac states, near the Γ point, is shown in Fig. 4(b) in a frontal view of the ribbon, i.e., looking at the ribbon infinite length. The topological edge states are distributed near the edge sites and with the penetration of a few unit cells inside the InBi-F nanoribbon. States are present within the SrTe substrate because of the dangling bond states present due to the artificially terminated SrTe substrate.

Since the edges are symmetric with respect to the center of the nanoribbon, the Dirac states are degenerate and spin-momentum locked. The spin projection of the edge states was calculated via the spin polarization vector, $P_n(k) = \langle u^{\sigma}_{nk}|\sigma|u^{\sigma}_{nk}\rangle$, where $|u^{\sigma}_{nk}\rangle$ are the *ab initio* Bloch states, and $\sigma = (\sigma_x,\sigma_y,\sigma_z)$ is the Pauli matrix vector. For a $\delta k$ close to the Γ point, we determined the spin projections $P_{x,n}$, $P_{y,n}$, and $P_{z,n}$, where for all states, 1–4, shown in Fig. 4(a), the $P_{x,n}$ and $P_{y,n}$ projections are negligible, with only the $P_{z,n}$ component remaining. A similar behavior was observed by Seixas *et al.* for the edge states in a germanane nanoroad [37]. The states above the Dirac point near Γ, energy bands 1 and 2 indicated in Fig. 4(b), have opposite spin polarizations and are localized on opposite edges of the ribbon. Furthermore, by inspecting states localized on the same edge, we find that they exhibit opposite spin polarizations, i.e., $\psi^{\uparrow}_{\Gamma-\delta k}$ and $\psi^{\downarrow}_{\Gamma+\delta k}$; thus, although lying on the same edge, backscattering processes are not allowed ($\psi^{\uparrow}_{\Gamma-\delta k} \nleftrightarrow \psi^{\downarrow}_{\Gamma+\delta k}$). The same applies to bands 3 ($\psi^{\downarrow}_{\Gamma-\delta k}$) and 4 ($\psi^{\uparrow}_{\Gamma-\delta k}$), as well as to the electronic states below the Dirac crossing, near the Γ point. These are main characteristics of quantum spin Hall insulators.

Finally, we also investigated multilayer systems with 2D topological insulators, composed of 2D TI layers sandwiched between SrTe layers such as the heterostructure schematically shown in Fig. 5(a). In this way, instead of passivating the top surface of the 2D InBi with H or halogen species, another layer of the SrTe is grown on top of the InBi. In order to verify that the InBi layer retains its topological properties, we explicitly simulated the heterostructure displayed in Fig. 5(b). It consists of an InBi layer between 13 atomic layers of SrTe on the bottom and 10 atomic layers on top of the InBi layer. The out-of-plane lattice parameter and atomic positions were fully relaxed.

The band structure of the SrTe/InBi/SrTe heterostructure, without SOC, is shown in Fig. 5(c). We can see an $s$-$p$ band inversion around the Fermi level. When SOC is included [see Fig. 5(d)], a nontrivial band gap appears at Γ, revealing that this heterostructure is also characterized by the presence of a 2D TI, the same behavior presented by the systems with hydrogen and halogens decorating the top surface. From these results, we conclude that we can create heterostructures based on III-Bi 2D TIs presenting large 2D nontrivial band gaps. This approach would be more robust, in practice, than having a freestanding InBi layer, as described by other authors, or even a single layer passivated with H or halogens. We believe that these results constitute a new route to the growth and use of 2D quantum spin Hall insulators in practical applications. The III-Bi layers could be deposited or grown on SrTe substrates using various epitaxial growth techniques, such as molecular beam epitaxy and chemical vapor deposition. For SrTe/III-Bi/SrTe structures, perhaps pulsed laser deposition would be more appropriate due to the flexibility regarding the number of different species present in the growth chamber, as the deposition of a SrTe top layer would be required to cap the III-Bi layer. In all, the growth or deposition will be facilitated by the small lattice mismatch between the III-Bi and the SrTe substrate and by the ultrathin layer thickness of the III-Bi layer.

## IV. CONCLUSIONS

In summary, we show that III-V bismuth–based 2D materials grown on anion-terminated SrTe(111) are 2D topological insulators when the exposed surface is decorated with hydrogen or halogens. All systems studied here exhibit large nontrivial band gaps, ranging from 0.15 to 0.72 eV. Our calculations show that Γ-centered 1D Dirac helical edge states appear on the edges of nanoribbon structures, and these states are protected by time-reversal symmetry. More importantly, when both sides of the 2D material are sandwiched by SrTe layers, the topological phases are still present, opening a new route to the building of devices based on 2D quantum spin Hall insulators.

## ACKNOWLEDGMENTS

This work was supported by the Brazilian agencies FAPESP, CNPq, and CAPES. A.J. acknowledges financial support from the U.S. DOE. We also would like to acknowledge computing time provided on the Blue Gene/Q supercomputer supported by the Research Computing Support Group (Rice University) and Laboratório de Computação Científica Avançada (Universidade de São Paulo), and the Extreme Science and Engineering Discovery Environment (XSEDE), which is supported by National Science Foundation Grant No. ACI-1053575. Finally, we acknowledge Dr. Soluyanov for sharing the code to calculate the Wannier charge centers in the VASP code.

[1] C. L. Kane and E. J. Mele, Phys. Rev. Lett. **95**, 226801 (2005).
[2] H. Min, J. E. Hill, N. A. Sinitsyn, B. R. Sahu, L. Kleinman, and A. H. MacDonald, Phys. Rev. B **74**, 165310 (2006).
[3] Y. Yao, F. Ye, X.-L. Qi, S.-C. Zhang, and Z. Fang, Phys. Rev. B **75**, 041401 (2007).
[4] B. A. Bernevig, T. L. Hughes, and S.-C. Zhang, Science **314**, 1757 (2006).
[5] A. Kara, H. Enriquez, A. P. Seitsonen, L. C. L. Y. Voon, S. Vizzini, B. Aufray, and H. Oughaddou, Surface Sci. Rep. **67**, 1 (2012).
[6] C. C. Liu, W. X. Feng, and Y. G. Yao, Phys. Rev. Lett. **107**, 076802 (2011).
[7] J. E. Padilha, L. B. Abdalla, A. J. R. da Silva, and A. Fazzio, Phys. Rev. B **93**, 045135 (2016).
[8] Y. Xu, B. Yan, H.-J. Zhang, J. Wang, G. Xu, P. Tang, W. Duan, and S.-C. Zhang, Phys. Rev. Lett. **111**, 136804 (2013).
[9] H. Zhang, C.-X. Liu, X.-L. Qi, X. Dai, Z. Fang, and S.-C. Zhang, Nat. Phys. **5**, 438 (2009).
[10] W. Zhang, R. Yu, H.-J. Zhang, X. Dai, and Z. Fang, New J. Phys. **12**, 065013 (2010).
[11] L. B. Abdalla, J. E. Padilha, T. M. Schmidt, R. H. Miwa, and A. Fazzio, J. Phys. Condens. Matter **27**, 255501 (2015).
[12] L. Seixas, D. West, A. Fazzio, and S. B. Zhang, Nat. Commun. **6**, 7630 (2015).
[13] E. Frantzeskakis, S. Pons, and Marco Grioni, Phys. Rev. B **82**, 085440 (2010).
[14] D. V. Khomitsky and A. A. Chubanov, J. Exp. Theor. Phys. **118**, 457 (2014).
[15] F.-C. Chuang, L.-Z. Yao, Z.-Q. Huang, Y.-T. Liu, C.-H. Hsu, T. Das, H. Lin, and A. Bansil, Nano Lett. **14**, 2505 (2014).
[16] Y. Ma, X. Li, L. Kou, B. Yan, C. Niu, Y. Dai, and T. Heine, Phys. Rev. B **91**, 235306 (2015).
[17] R. R. Q. Freitas, F. de Brito Mota, R. Rivelino, C. M. C. de Castilho, A. Kakanakova-Georgieva, and G. K. Gueorguiev, J. Phys. Chem. C **119**, 23599 (2015).
[18] R. R. Q. Freitas, F. de Brito Mota, R. Rivelino, C. M. C. de Castilho, A. Kakanakova-Georgieva, and G. K. Gueorguiev, Nanotechnology **27**, 055704 (2016).
[19] J. E. Padilha, R. B. Pontes, T. M. Schmidt, R. H. Miwa, and A. Fazzio, Sci. Rep. **6**, 26123 (2016).
[20] Z.-Q. Huang, C.-H. Hsu, F.-C. Chuang, Y.-T. Liu, H. Lin, W.-S. Su, V. Ozolins, and A. Bansil, New J. Phys. **16**, 105018 (2014).
[21] F. Zhu, W.-J. Chen, Y. Xu, C.-L. Gao, D.-D. Guan, L. Canhua, D. Qian, S.-C. Zhang, and J.-F. Jia, Nat. Mater. **14**, 1020 (2015).
[22] Y. Xu, P. Tang, and S.-C. Zhang, Phys. Rev. B **92**, 081112(R) (2015).
[23] C. P. Crisostomo, L.-Z. Yao, Z.-Q. Huang, C.-H. Hsu, F.-C. Chuang, H. Lin, M. A. Albao, and A. Bansil, Nano Lett. **15**, 6568 (2015).
[24] L.-Z. Yao, C. P. Crisostomo, C.-C. Yeh, S.-M. Lai, Z.-Q. Huang, C.-H. Hsu, F.-C. Chuang, H. Lin, and A. Bansil, Sci. Rep. **5**, 15463 (2015).
[25] P. Hohenberg and W. Kohn, Phys. Rev. **136**, B864 (1964).
[26] W. Kohn and L. J. Sham, Phys. Rev. **140**, A1133 (1965).
[27] J. P. Perdew, K. Burke, and M. Ernzerhof, Phys. Rev. Lett. **77**, 3865 (1996).
[28] G. Kresse and J. Furthmüller, Phys. Rev. B **54**, 11169 (1996).
[29] G. Kresse and D. Joubert, Phys. Rev. B **59**, 1758 (1999).
[30] A. A. Soluyanov and D. Vanderbilt, Phys. Rev. B **83**, 035108 (2011).
[31] A. A. Soluyanov and D. Vanderbilt, Phys. Rev. B **83**, 235401 (2011).
[32] N. Marzari, A. A. Mostofi, J. R. Yates, I. Souza, and D. Vanderbilt, Rev. Mod. Phys. **84**, 1419 (2012).
[33] T. Ozaki, Phys. Rev. B **67**, 155108 (2003).
[34] G. Theurich and N. A. Hill, Phys. Rev. B **64**, 073106 (2001).
[35] J. Heyd, G. E. Scuseria, and M. Ernzerhof, J. Chem. Phys. **118**, 8207 (2003).
[36] J. Heyd, G. E. Scuseria, and M. Ernzerhof, J. Chem. Phys. **124**, 219906 (2006).
[37] L. Seixas, J. E. Padilha, and A. Fazzio, Phys. Rev. B **89**, 195403 (2014).